Investigating the Freezing-Thawing Hysteresis of Soils

YING *Yonghan*[1], TENG *Jidong*[1], DONG *Antai*[1,2], and SHENG *Daichao*[1,3]

[1]School of Civil Engineering, Central South University, Changsha 410075, China

[2]Missouri University of Science and Technology, Rolla 65409-0030, the United States

[3]School of Civil and Environmental Engineering, University of Technology Sydney, Sydney, NSW 2007, Australia

Abstract. The freezing-thawing characteristics of frozen soil are crucial for safe and reliable construction projects in cold regions. In this study, nuclear magnetic resonance (NMR) technology is employed to carry out freezing-thawing tests, aiming to explore the hysteresis behavior of soil during freezing and thawing. Three representative soil types (poorly graded sand, silt, and fat clay) are tested under different temperature modes to analyze their hysteretic characteristics of the soil freezing characteristic curve (SFCC). The results show that the hysteresis primarily occurs in the supercooling and rapid-decline stages, and the hysteresis loops of fat clay and silt are more distinct. The SFCC tests under different temperature modes reveal differences between the hysteresis of SFCC and that of the soil water characteristic curve (SWCC). Importantly, the supercooling phenomenon is identified as the main cause of this hysteresis. Based on this, we propose a theoretical model that incorporates the supercooling phenomenon into predictions of freezing-thawing hysteresis. By comparing with the measured data, this model can effectively capture all three stages of soil freezing-thawing hysteresis and particularly excel in predicting the supercooling and rapid freezing stages, with higher correlation coefficients and broader applicability. This study clarifies the critical role of supercooling in soil freezing-thawing hysteresis and builds a robust model for applications in cold-region engineering.

1 Introduction

Since Koopmans and Miller[[1]] first found the soil freezing-thawing hysteresis in the lab, many studies have studied this topic. Even though there is no unified understanding of its mechanism. Existing explanations fall into two categories: those borrowing from unsaturated soil drying-wetting hysteresis theories (e.g., pore-blocking, contact angle hysteresis, and pore geometry theories[[2]]) and those specific to freezing-thawing hysteresis (e.g., free energy barrier and pore water supercooling theories[[3]]). However, these mechanisms have limitations. The former overlook ice formation in soil pores, and the latter lack micro-scale verification.

There are three main types of mathematical models. Empirical models are overly dependent on experimental data and lack a clear physical basis[[4]]. SWCC-based models inadequately capture the complex ice-water phase transitions affected by supercooling. Thermodynamic models focus on individual pores and ignore interactions between pores in the soil structure[[3]]. Although freezing-thawing hysteresis exhibits similarities with drying-wetting hysteresis, there exist essential discrepancies in physics. Additionally, although hypotheses about ice-water phase change can be proposed from a thermodynamic perspective, they are limited to the microscopic scale and lack validation.

This study applies NMR to measure unfrozen water content changes during freezing-thawing cycles, obtain SFCC data, and compare differences between SFCC and SWCC hysteresis mechanisms. It reveals the main cause of freezing-thawing hysteresis, and a new model considering supercooling is proposed. Validation against experimental data confirmed the model's effectiveness and reliability. The innovation lies in clarifying that supercooling is the main cause of soil freezing-thawing hysteresis and establishing a simple, physically meaningful model for cold-region engineering applications.

2 Experimental Study

2.1Test equipment, materials, and procedure

The laboratory tests are performed using the Nuclear Magnetic Resonance Geotechnical Microstructure Analyzer (NMRC12-010V), which is jointly developed by Central South University and Suzhou Niumag Analytical Instrument Corporation. The apparatus consists of three parts: an operating system, a magnetic field, and a temperature control system (see Figure 1(a)). The operating system is utilized to set test parameters and record experimental data. The magnetic field is used for magnetization, resonance, and relaxation of hydrogen protons.

The temperature control system regulates the sample temperature, comprising an exchange cabinet and a

Corresponding author: jdteng@csu.edu.cn

chiller. A detailed schematic of the test unit is shown in Figure 1(b), where a cylindrical sample with a diameter of 9 mm and a height of 10 mm can be placed inside the sample cell. A temperature sensor is positioned at the top of the sample to record temperature changes in real time. Both the test cell and the cold bath vessel are sealed with a sealing film to prevent external water vapor from affecting the test.

(a) main component

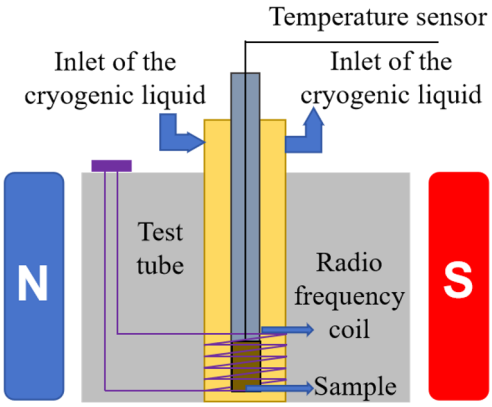

(b) schematic diagram of the test chamber

Fig. 1. Diagram of NMR apparatus

Three representative soils were selected as experimental materials: (1) poorly graded sand, mainly composed of quartz with a particle size ranging from 0.075 to 1.0 mm, (2) silt sampled from Hohhot Baita International Airport, and (3) fat clay. Detailed physical properties are shown in Table 1. All samples underwent the main freezing-thawing process from 248.15 K to 283.15 K. The temperature intervals of the main freezing process (from 272.15 K to 266.15 K) and the main thawing process (from 270.15 K to 273.15 K) were set to 0.5 K. After the main freezing-thawing process, the samples also underwent a scanning freezing-thawing process from 265.15 K to 272.15 K. Each temperature point was maintained for 30 minutes to reach thermal equilibrium. After the experiment, the signal data of the samples were analyzed to obtain the unfrozen water content at each temperature point.

Table 1. Physical properties of the experiment materials.

Soil type	Specific gravity	Liquid limit (%)	Plastic limit (%)	Optimum water content (%)	Maximum dry density (g/cm3)
Poorly graded sand	2.65	/	/	/	1.65
Silt	2.69	23.18	19.56	14.20	1.90
Fat clay	2.69	57.0	26.00	15.31	1.82

Table 2. Test conditions.

Soil type	Dry density (g/cm^3)	Measured water content (g/g)
Poorly graded sand	1.6	0.196 (Saturated)
Silt	1.8	0.237 (Saturated)
Fat clay	1.8	0.263 (Saturate)

2.2 Experimental results and analysis

2.2.1 Hysteresis of main curves

The main freezing process' soil freezing characteristic curve (SFCC) has three stages: supercooling, rapid decline, and residual stability. The main thawing process' SFCC includes stability, slow thawing, and rapid thawing, with no supercooling during thawing. The hysteresis of the main freezing-thawing curves is mainly in the supercooling and rapid-decline stages, and less obvious in the residual-stability stage. Fat clay and silt have more distinct top-wide and bottom-narrow hysteresis loops compared to sand because of their wider pore-size distributions and slower SFCC changes during thawing.

When comparing the slopes of freezing and thawing curves, it can be found that the freezing curve declines faster overall. The freezing curve declines sharply when the soil temperature drops below T_{sc}. The thawing curve rises gradually before approaching T_m and only accelerates when the temperature is close to T_m. This differs from the approximate parallelism of SWCC's wetting and drying curves, meaning the SWCC's hysteretic mechanism can't explain the soil's freezing-thawing hysteresis. Pore water freezing needs nucleation and the Gibbs-Thomson effect. In the supercooling stage, large-pore liquid water cannot freeze due to the lack of nucleation. After nucleation, pore water freezes rapidly, accelerating the overall freezing.

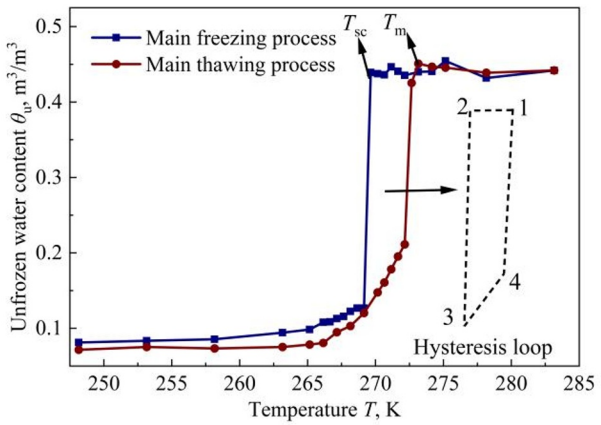

(a) Poorly graded sand

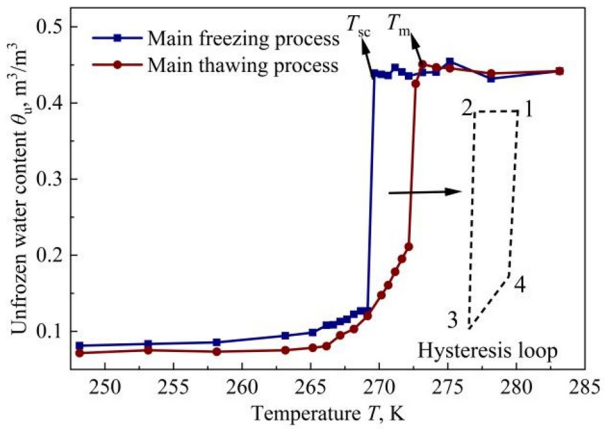

(b) Silt

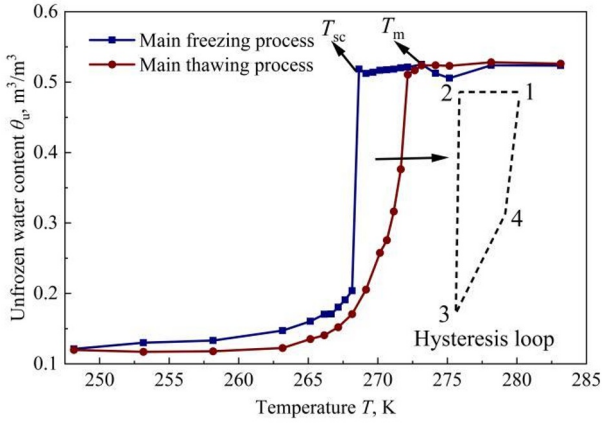

(c) Fat clay

Fig. 2. Freezing-Thawing Characteristic Curve

2.2.2 Effect of the temperature mode

The influence of temperature patterns on freezing-thawing hysteresis is shown in Fig. 3. The scanning thawing curve roughly follows the path of the main thawing curve, while the scanning freezing curve is slightly higher than the scanning thawing curve. It is noted that there is no supercooling above T_{sc} as residual ice from incomplete thawing eliminates it. Supercooling occurs in subsequent freezing after thawing above T_m, the ice in the soil will be completely melted and the supercooling will be present in the subsequent freezing process, but this is essentially already a main freezing-thawing process.

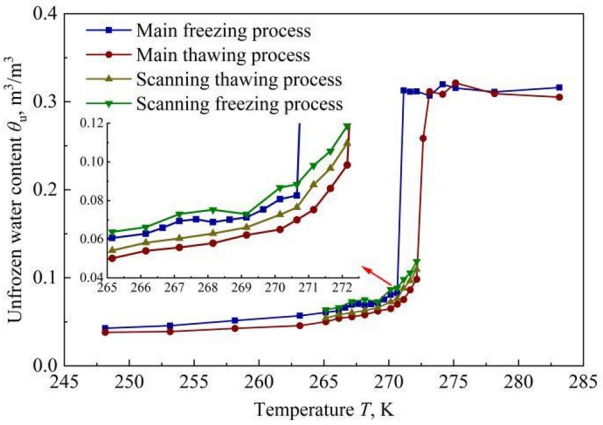

(a) Poorly graded sand

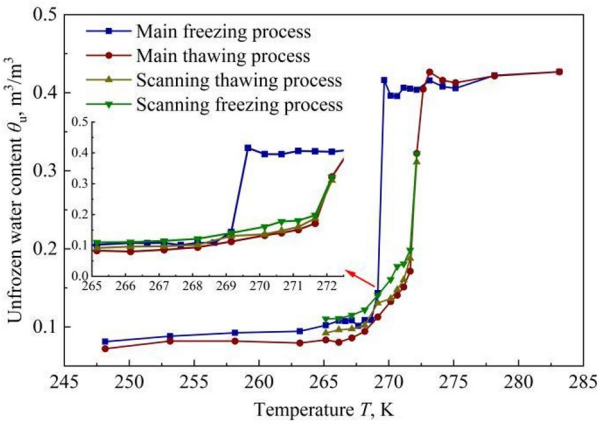

(b) Silt

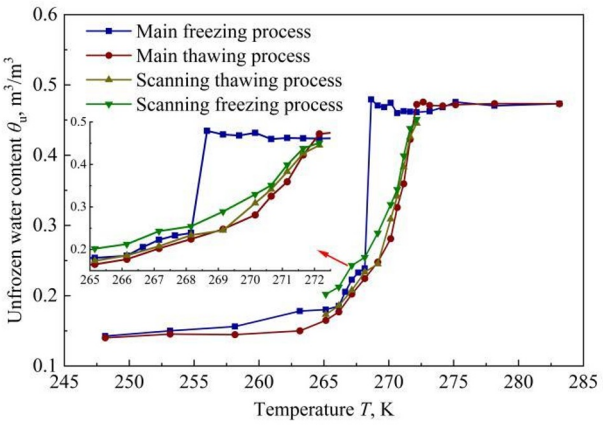

(c) Fat clay

Fig. 3. SFCCs associated with the main and scanning freezing-thawing processes

Fig. 4 shows that the hysteretic level of the main process exhibits a unimodal pattern, with maximum values exceeding 0.5 for all three soils and the largest for poorly graded sand, the reason may be that the pore size

distribution of poorly graded sand is more concentrated, resulting in steeper and parallel SFCCs during freezing and thawing.

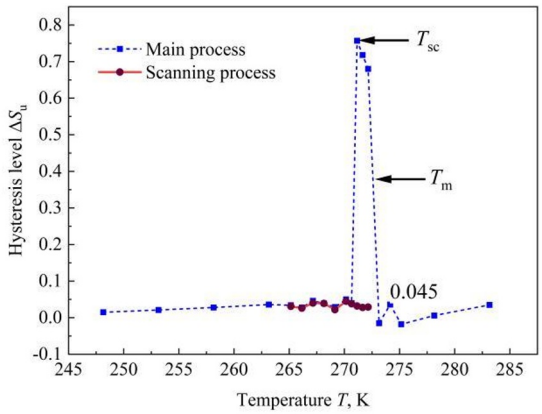

(a) Poorly graded sand

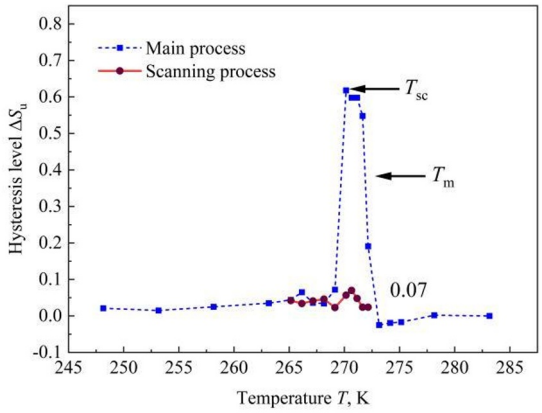

(b) Silt

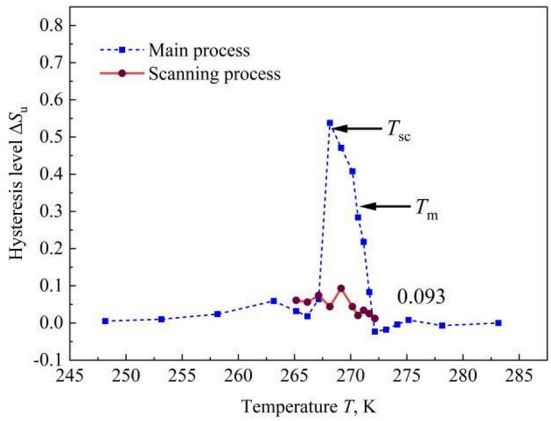

(c) Fat clay

Fig. 4. Variation of the hysteresis level in terms of the temperature during the main and scanning freezing-thawing processes

The hysteretic level of the scanning process is very low, with the maximum values lower than 0.1 for all three soils. This fact indicates that the hysteretic behavior during the scanning process is less significant than that during the main process. Moreover, the absence of supercooling during the scanning freezing process is the main reason for the insignificant hysteresis.

Some factors may have specific impacts on freezing-thawing hysteresis, such as pore blocking, geometry effects, and end free-energy barriers. During wetting-drying processes, water-air interfaces are blocked by small pores. However, in freezing-thawing, ice forms randomly. In scanning, incompletely thawed ice weakens pore-blocking. These factors cannot explain the differences in Fig. 3. Thus, it can be concluded that supercooling is the primary reason for freezing-thawing hysteresis. Additionally, due to the absence of supercooling in the scanning process, its hysteresis effect is not significant. This implies that approximating scanning curves with the main thawing curve introduces only minimal errors, which provides a clear and concise insight into the application of SFCC hysteresis.

3.Theoretical Analysis

3.1 Analysis of Pore Water Supercooling

According to the classical nucleation theory, the nucleation barrier can only be overcome when the temperature T drops to the supercooling temperature T_{sc}. At this time, ΔT is defined as the supercooling degree $\Delta T_{sc} = T_{eq} - T_{sc}$.

$$\Delta T_{sc} = \frac{N_A \Omega_s}{L_{wi}} \left[\frac{16\pi T \sigma_{il}^3}{3k \ln(K)} \right]^{1/2} f(\theta)^{1/2} \quad (1)$$

After substituting the values of each parameter in Table 3, it can be further simplified as:

$$\Delta T_{sc} = 32.51 f(\theta)^{1/2} \quad (2)$$

The contact angle θ is governed by the physicochemical properties of the particle surface and directly dictates the degree of supercooling. Through inversion fitting, the proposed contact angle ranges for different soil types are 14° to 22° for sand, 18° to 26° for silt, and 20° to 28° for clay. Specifically, sand exhibits larger pores and stronger surface hydrophilicity, resulting in a smaller contact angle and higher nucleation efficiency; Clay has finer pores and more surface active sites, leading to a larger contact angle and more significant supercooling effects.

Table 3. Input parameter values for determining the supercooling degree.

Parameter	Symbol	Value	Unit
Avogadro's constant	N_A	6.02×10^{23}	1/mol
Volume of a water molecule in an ice embryo	Ω_s	2.99×10^{-29}	m^3
Latent heat of water freezing	L_{wi}	6.01×10^{3}	J/mol
Surface free energy between ice and liquid	σ_{il}	3×10^{-2}	J/m^2
Boltzmann constant	k	1.38×10^{-23}	J/K
Nucleation rate factor	K	10^{36}-10^{42}	$1/(m^3\cdot s)$

3.2 Freezing-thawing hysteresis model

To develop a new SFCC hysteresis model, some assumptions are made as follows:

(1) The soil is assumed to be saturated, i.e., the air phase within voids is neglected.

(2) The soil pores are regarded as a collection of capillary tubes with varying sizes arranged in descending order: r_0, r_1, r_2, …, r_{min}.

(3) The thawing process is assumed to be approximately equivalent to the wetting process of unsaturated soil.

The SFCC during the Thawing Branch is expressed as:

$$\theta_{uT} = \theta_r + (\theta_s - \theta_r) / \left[1 + \left(\frac{\Delta T}{\Delta T_m} H(\Delta T) \right)^n \right]^m \quad (3)$$

where H(x) represents the Heaviside function, which takes 0 for x < 0 and 1 for x ≥ 0.

The SFCC during the Freezing Branch is expressed as:

$$\begin{cases} \theta_{uF} = \theta_r + (\theta_s - \theta_r) / \left[1 + \left[\frac{\left[\Delta T - \Delta T_{sc} \left[1 - \mathrm{CDF}(T) \right] \right] H(\Delta T - \Delta T_{sc})}{\Delta T_m} \right]^n \right]^m \\ \mathrm{CDF}(T) = \frac{1}{2} \left(1 - \mathrm{erf} \left(\frac{T - \left(T_f - \frac{\Delta T_{sc}}{2} \right)}{\sqrt{2} \cdot \frac{\sqrt{2} \Delta T_{sc}}{8}} \right) \right) \end{cases} \quad (4)$$

where CDF(T) represents the cumulative distribution function of the standard normal distribution[[5]]. The expression $T_c = T_f + \Delta T_{sc}/2$ denotes the mean temperature, and the term $\sigma_c = \sqrt{2}\,\Delta T_m/8$ signifies the standard deviation. The term (1-CDF(T)) represents the rapid freezing induced by supercooling.

3.3 Model Validation

Measured data from this study were used to validate the model. Water cont ent was converted to unfrozen water saturation(S_u) for comparison. Models by Zhou et al.[[6]] based on SWCC hysteresis and Petrov and Furó's[[3]] thermodynamic model were chosen for comparison.

In the proposed model, m, n, and ΔT_m were determined by fitting thawing data, ΔT_{sc} was calculated, and θ was obtained by least-squares fitting. The parameter λ in Petrov and Furó's model was fitted to the data.

Compared with experimental data and existing models, the proposed model better captures the hysteretic behavior at all three stages, particularly during the initial phase change and rapid phase change stages. Comparing the SFCCs of the three soils in Figure 5, it is found that Tm gradually decreases from sand to clay. This is attributed to the absence of supercooling during the thawing process, and Tm correlates with pore size.

Additionally, as shown in Figure 5(a), the predicted curves for sand using the proposed model exhibit nearly parallel behavior during the rapid phase-change stage. In contrast, the slopes of the soil freezing characteristic curves for silt and fat clay during the freezing process in Figures 5(b) and (c) increase significantly compared to the thawing process. This observation is consistent with the experimental findings. The results obtained indicate that the consideration of the rapid phase-change stage by the proposed model is reasonable.

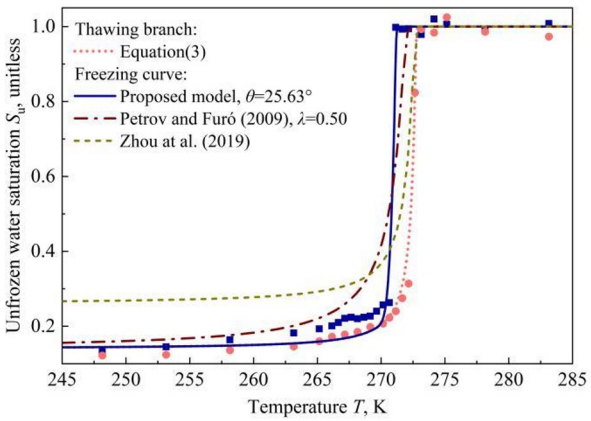

(a) Poorly graded sand

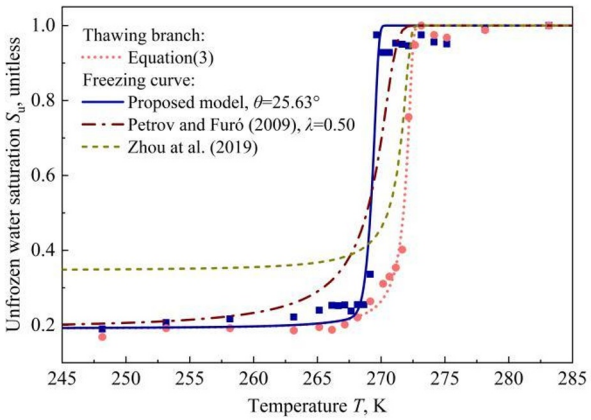

(b) Silt

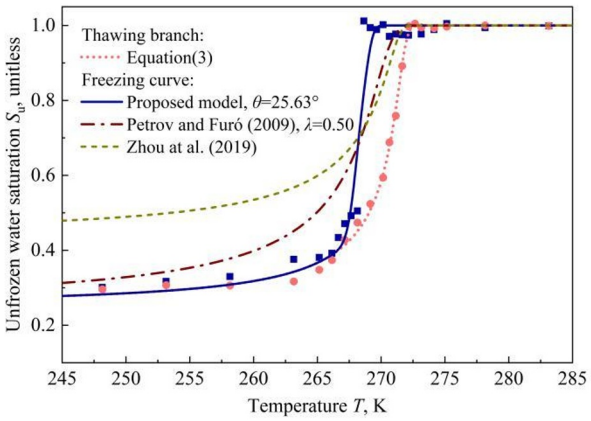

(c) Fat clay

Fig. 5. Comparison of the predicted and measured SFCCs for different soil types

4 Conclusions

This study uses NMR techniques to explore soil freezing-thawing hysteresis behavior. Lab tests were conducted to clarify the underlying hysteresis mechanism, revealing that freezing lags behind thawing, and that the freezing curve drops more sharply due to

supercooling's inhibition on pore water freezing. SFCC tests with different temperature modes highlight differences between SFCC and SWCC hysteresis. Unlike SWCC, the main branches of SFCC are not parallel. Scanning curves closely follow the main thawing branch, and scanning-process hysteresis is minimal, which is unlike the parallelism of SWCC wetting-drying curves. These findings challenge traditional SWCC-based hysteresis theories and reinforce the critical role of supercooling.

Based on substable heterogeneous nucleation theory, a new freezing-thawing hysteretic model is developed which relates supercooling degree to contact angle, considers supercooling's effects in different stages, combines nucleation barrier and fluid flow influences, has a simple form and clear physical meaning, and performs better than previous models in predicting supercooling and rapid freezing stages.

This research was supported by the National Natural Science Foundation of China (No.52178376), National Key R&D Program of China (No.2022YFB2603301), Natural Science Foundation of Hunan Province (2022JJ10076).

References

[1]. Koopmans, R. W. R., and Miller, R. D., Soil Sci. Soc. Am. J. **30**, 680–685 (1966).
[2]. Bittelli, M., Flury, M., and Campbell, G. S., Water Resour. Res. **39** (2), SBH111–SBH1110 (2003).
[3]. Petrov, O. V., and Furó, I., Prog. Nucl. Magn. Reson. Spectrosc. **54** (2), 97–122 (2009).
[4]. Liu, Z., and Yu, X., Transportation Res. Rec. **2349**, 93–99 (2013).
[5]. Lu, N., J. Geotech. Geoenviron. Eng. **10** (142), 04016051 (2016).
[6]. Zhou, Y., Zhou, J., Shi, X., and Zhou, G., Cold Reg. Sci. Technol. **157**, 215–223 (2019).
[7]. Teng, J., Zhong, Y., Zhang, S., and Sheng, D., Cold Reg. Sci. Technol. **181**, 103178 (2021).
[8]. Teng, J., Kou, J., Yan, X., Zhang, S., and Sheng, D., Cold Reg. Sci. Technol. **170**, 102928 (2020).
[9]. Teng, J., Liu, J., Zhang, S., and Sheng, D., Acta Geotech. **15** (11), 3307–3320 (2020).
[10]. .Teng, J., Liu, J., Zhang, S., and Sheng, D., Géotechnique 73 (12), 1100–1111 (2022)